# FLOW PERMEATION ANALYSIS OF BOVINE CERVICAL MUCUS

D. F. KATZ
*Department of Obstetrics and Gynecology, School of Medicine, University of California, Davis, California 95616*

P. Y. TAM AND S. A. BERGER
*Department of Mechanical Engineering, University of California, Berkeley, California 94720*

G. F. SENSABAUGH
*School of Public Health, University of California, Berkeley, California 94720*

ABSTRACT Geometrical properties of the microstructure of whole bovine cervical mucus were studied. An experimental technique was developed for measuring the flow of fluid through the mucus microstructure in response to application of a prescribed external pressure gradient. The data obtained were analyzed in conjunction with a mathematical model of the hydrodynamics of the flow-permeation process. The sizes of typical interstices within the microstructure were calculated to be of the order of 1 $\mu$m, with typical macromolecular filament diameters being of the order of 100 Å. These dimensions were interpreted as representative of an equivalent network giving rise to measured flow permeability. The values of filament size showed a strong experimental correlation with the solids content of the mucus.

## INTRODUCTION

The uterine cervix is an anatomical juncture situated at the posterior end of the vagina. In many mammals insemination occurs within the vagina; the cervix thus functions as the initial passageway through which spermatozoa migrate, en route to the site of fertilization in the oviduct. In a number of these species, including primates and ruminants, the cervical canal is filled with mucus that is generally similar to that of the respiratory tract. The cervical mucus can be regarded as consisting of a solid phase (mucin) and a liquid phase (plasma). The liquid phase consists of soluble proteins, low molecular weight carbohydrates and electrolytes, and comprises 95–99% or more of the whole mucus (Blandau and Moghissi, 1973). The solid phase is a polydisperse system of fibrous glycoprotein macromolecules (Gibbons and Mattner, 1966; 1971).

The whole mucus possesses a remarkable set of rheological and other biophysical properties that are intimately associated with its physiological function. This function involves the admission of morphologically normal, vigorous spermatozoa into the cervix, and their subsequent distribution and upward migration (Davajan et al., 1970; Blandau and Moghissi, 1973; Elstein et al., 1973; Overstreet and Katz, 1977). Viscoelastic and other rheological properties of human and bovine cervical mucus have been described and related to cervical function (e.g. Nakamura et al., 1973; Eliezer, 1974; Wolf et al., 1977; Tam et al., 1980). These studies have characterized the mucus on a scale that is large compared with the size of a swimming spermatozoon. Certain inferences, primarily qualitative, can be drawn between the macroviscoelastic behavior of the mucus and the local properties of the microstructure (e.g. Lutz et al., 1973). However, relatively little attention has been devoted to the specific microarchitectural properties of the mucus that modulate the movements of spermatozoa within it. In this regard, the geometry of the mucin network, i.e., the sizes of the filaments and of the interstices between them, is of paramount importance (Katz and Berger, 1980). Using scanning and transmission electron microscopy, the mucus microstructure has been made visible (Singer and Reid, 1970; van Bruggen and Kremer, 1970; Chretien et al., 1973; Zaneveld et al., 1975). The conflicting pictures of the microstructure resulting from these studies seem to be associated with different methods of specimen dehydration and fixation (Chretien, 1977). Mucus contracts during these processes, and is not sheared uniformly because of its adherence to solid surfaces. The loss of soluble electrolyte may also change the dimensional organization of the microstructure. Consequently, the quantitative and even qualitative relationships between the photomicrographs of electron microscopy and the nature of the microstructure of whole mucus are not established.

Dr. Tam's current address is the Center for Bioengineering, University of Washington, Seattle, Washington.

The present study was designed to consider the geometry of the mucus microstructure in its native gel state. The forced microhydrodynamic permeation of mucus plasma through the mucin network was investigated. The relationship between the flow rate of this permeation and the applied pressure gradient, i.e., the mucus permeability, is a reflection upon the known viscosity of the plasma and the geometry of the network. Experimental measurements were performed, and then applied to a mathematical model of the hydrodynamics of the flow-permeation process. Typical mucin filament sizes and spacings, characteristic of a hydrodynamically equivalent microstructure, were then computed.

## METHODS

### Experimental Apparatus

The apparatus used to measure permeability of mucus to its own plasma consists of the following principal components (Fig. 1):

(*a*) A mucus aliquot holder is an open glass tube, at the bottom of which is cemented a stainless steel screen; a 0.8-$\mu$m millipore filter is placed upon the upper surface of the screen. The size of filter was selected to retain the mucus gel while allowing plasma to flow through it.

(*b*) In the back pressure system a syringe and an "upstream" valve apply and maintain a given pressure (above atmospheric), which is monitored by the water manometer; a rubber stopper provides an air-tight seal to the mucus aliquot holder.

(*c*) The flow meter consists of a 100-$\mu$l Hamilton syringe and a "downstream" valve.

The flow rate of plasma at each applied back pressure is obtained in the following steps:

(*a*) That portion of the flow system downstream of the millipore filter is "primed" with either mucus plasma or saline solution. Using the downstream valve, the fluid meniscus is positioned at an initial mark on the Hamilton syringe.

(*b*) A mucus aliquot is loaded carefully into the aliquot holder so that it rests on the filter. The exact height of the mucus plug is measured. Mucus plasma or saline are added gently on top of the mucus. Because the mucus plug is thus completely surrounded by plasma and the aliquot holder, the hydration of the plug remains constant during a measurement sequence.

(*c*) The back pressure system is connected to the holder by inserting the rubber stopper. A specific back pressure is applied by displacing the syringe plunger. Closing the upstream valve maintains the specific pressure.

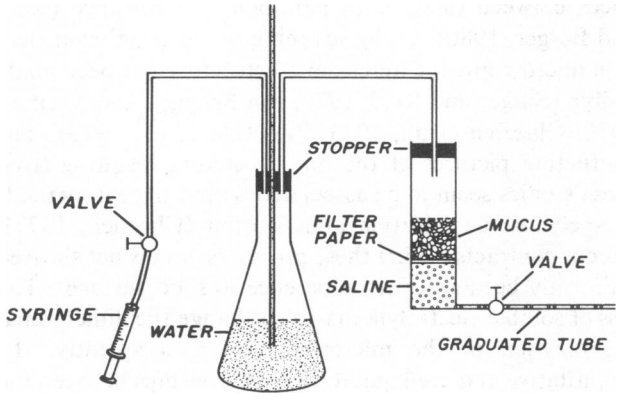


FIGURE 1 Flow-permeation system.

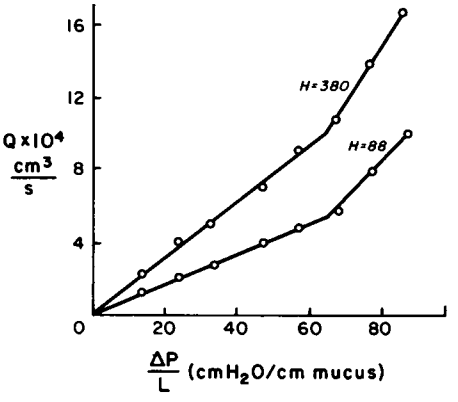


FIGURE 2 Typical flow-permeation plots for two samples of bovine cervical mucus. *H*, native hydration.

(*d*) Simultaneously, the downstream valve is opened and a stopwatch is started. After the fluid meniscus has traversed a specific distance indicated by the grid marks on the Hamilton syringe, the stopwatch is stopped. These measurements determine the flow rate at which plasma is expressed from the whole mucus. A plot of flow rate vs. applied pressure gradients is then obtained for each sample. A typical plot is shown in Fig. 2.

### Materials

Bovine cervical mucus was obtained from healthy Holstein dairy cows. A sterile glass pipette, 40-cm long, 0.5-cm i.d., 0.8-cm o.d., was inserted into the external cervical os, and mucus was withdrawn by gentle suction. The pipette was then placed in a vertical position and the mucus was allowed to run out and into a 10-ml collection tube, 1.5-cm i.d. Gentle back pressure was applied to the pipette, to facilitate the expiration process. The collection tube was then sealed and placed in a 4°C environment. Mucus samples containing any evidence of pus or blood were not included in this study. The estrous cycle phase of each donor cow was ascertained by intrarectal palpation of the ovaries and reproductive tract. Behaviorial evidence of estrous was also taken into account. Mucus samples in this study were determined to have been collected during a 3-d peri-ovulatory period. All experiments were performed within 24 h of mucus collection.

### Theoretical Model

Mathematical analysis of the experimental data focused upon the relationship between the applied pressure difference across the mucus sample, $\Delta P$, and the resulting volumetric flow rate of expressed mucus plasma, $Q$. This relationship depends upon the size and shape of the mucus sample, in our case the length of the mucus column, $L$, the cross-sectional area $A$, the viscosity of the plasma, $\eta$, and the resistance offered by the microstructure, $\mathcal{R}$. Thus,

$$Q = A\Delta P/\eta\mathcal{R}L. \quad (1)$$

Recasting this equation into the familiar form of Darcy's Law, one obtains:

$$J = Q/A = k\Delta P/\eta L \quad (2)$$

where $k = 1/\mathcal{R}$ is the permeability coefficient, or flow conductivity. The resistance $\mathcal{R}$ can be related specifically to a geometrical model of the microstructure. The mathematical expression for $\mathcal{R}$ was obtained by introducing the concept of a quintessential "cell" within the mucus, the net value of $\mathcal{R}$ being the sum over all such cells.

In the model here a typical fluid cell (Fig. 3) is cylindrical, with a shear-free fluid boundary of radius $R$. The hydrodynamic interaction with the filaments of adjacent cells is taken into account by the shear-free

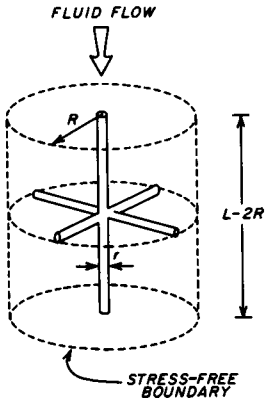


FIGURE 3 Typical cell.

nature of the outer boundary and its radius, the latter depending upon the mucus-solids content. Cell models akin to the one proposed here have been used to accurately model convection plus diffusion in particulate systems (Yaron and Gal-Or, 1971) as well as diffusion alone within bovine cervical mucus (Katz and Singer, 1978). The core of each cell is occupied by cylindrical filaments. Mucus plasma is represented by the fluid surrounding the filaments. If the network of macromolecules is considered to be random, on the average, then for every one filament whose longitudinal axis is oriented along the direction of flow, there are two perpendicular ones. The radius of these filaments is $r$. The cells are stacked to form an overall cuboidal structure (Fig. 4).

To achieve a regular cuboidal assemblage of fluid cells, the following geometrical constraints are imposed:

(*a*) The lengths of the parallel and perpendicular filaments are equal to $L$; therefore, the separation between the parallel filaments of neighboring cells is $L$.

(*b*) $R$, the radius of the fluid cell is equal to $L/2$.

(*c*) The length of the cell is $L$.

Having assumed such a geometrical model, one can proceed to calculate the hydrodynamical resistance of such a network to fluid flow. In this case, hydrodynamical analysis (see Appendix) gives the resistance $D$ per unit length of the cell as

$$D = 2\pi\eta U\,[(5 - \epsilon^2)/(-\ln\epsilon + \epsilon^2 - \epsilon^4/4 - 0.75)], \quad (3)$$

where $U$ is the effective velocity of the permeating fluid, and $\epsilon = r/R$ is the ratio of filament radius to cell radius. The total hydrodynamical resistance in the cell can be related to the back pressure gradient necessary to force fluid through it at a given rate $U$:

$$\Delta P/L = D/\pi(R^2 - r^2)$$
$$= [2\eta U/R^2(1 - \epsilon^2)]\,[(5 - \epsilon^2)/(-\ln\epsilon + \epsilon^2 - \epsilon^4/4 - 0.75)]. \quad (4)$$

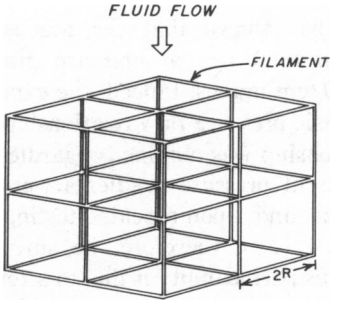


FIGURE 4 Cubic lattice model.

Inasmuch as $Q/A = U$, the flow conductivity $k$ can be readily identified from Eq. 4 as

$$k = \tfrac{1}{2}R^2(\epsilon^2 - 1)\,[(-\ln\epsilon + \epsilon^2 - \epsilon^4/4 - 0.75)/(5 - \epsilon^2)]. \quad (5)$$

In Eq. 4, the quantities $\Delta P/L$, $U$, and $\eta$ can be directly measured in each experiment. The viscosity of the mucus plasma is $\eta = 1.0$ cP at 21°C, (unpublished observations). There remain the unknowns $r$ and $R$. In arriving at Eq. 4, the implicit assumption made was that there is little hydrodynamical interaction between the parallel and perpendicular filaments; consequently, the drags due to the individual filaments are simply additive. This is justified, to a first approximation, since the ratio of interstitial spacing $R$ to $r$ is of the order of 20–40.

A second expression containing $r$ and $R$ can be obtained by determining the mucus nondialyzeable solids content. Experimentally this was measured by initial weighing of an aliquot of mucus sample, dialysis against distilled water for 48 h, and then lyophylization and weighing of the dry lyophylate. The degree of mucus hydration, $H$ = (weight of water)/(weight of solid), can be related to $r$ and $R$ using the same geometrical model of the mucus microstructure as introduced previously. For the cubic lattice, the relationship is (see Appendix)

$$r/R = [3(H + 1)]^{-1/2}. \quad (6)$$

Eqs. 4 and 6, with experimental measurement of $Q$, $\Delta P$, $L$, $H$, and $\eta$, are, therefore, sufficient to compute the filament radius $r$ and spacing $2R$.

## RESULTS

Results obtained from this study can be divided into the categories of experimental and derived results.

### Experimental

For each mucus sample, measurements were made of plasma flow rates that corresponded to several applied back pressures. All measurements in this study were performed at room temperature (21° ± 1°C). A typical flow pressure curve is shown in Fig. 2. Note that there is a change in the slope of the curve at pressure gradients in the range of 40–60 cm $H_2O$/cm mucus. In each of these flow regimes, the flow rate is directly proportional to the applied pressure gradient. Their relationship, for both regimes, was fitted to a linear regression line with a linear correlation coefficient $r > 0.90$ for all samples tested ($P \leq 0.05$). A flow conductivity (or Darcy's coefficient) $k$, corresponding to each slope of the flow-pressure curve, can be calculated. For flow rates in units $cm^3/s$ and pressure gradients in units dynes $cm^{-2}$/cm mucus, the flow conductivity has the units: $cm^4\ s^{-1}$/dyne. Figs. 5 and 6 show a plot of flow conductivity vs. native hydration of mucus for the initial pressure range of $0.5 \times 10^{-9}$ to $3 \times 10^{-8}$, and for the higher pressure range of $10^{-8}$ to $6 \times 10^{-8}$. Note that there is a two to threefold increase in the flow conductivity between these two pressure ranges. Repeated testing of individual plugs of mucus revealed no hysteresis in these biphasic flow-pressure plots.

### Derived

According to the model proposed, we can calculate from the values of the permeability constant and hydration of

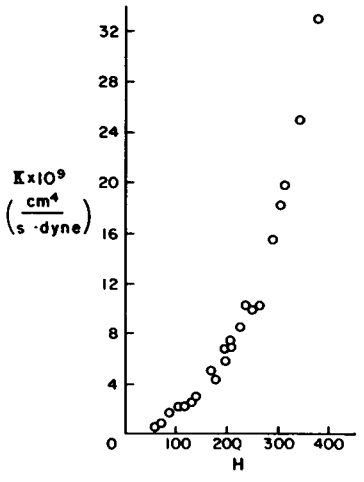


FIGURE 5 Distribution of flow conductivity $k$ at low-pressure regime of flow curve vs. native hydration for bovine cervical mucus.

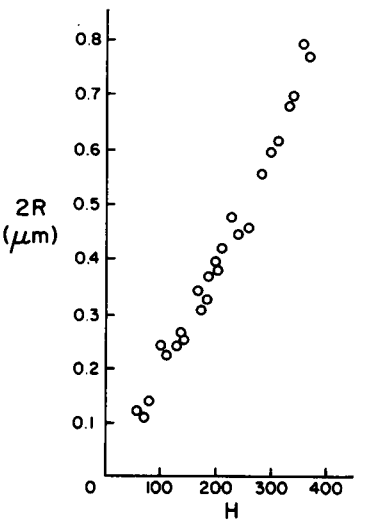


FIGURE 7 Distribution of equivalent pore sizes, $2R$, calculated from flow-permeation data, vs. native hydration, $H$, for bovine cervical mucus.

each mucus sample a value of interstitial spacing $2R$ and filament radius $r$. This is achieved by obtaining the value of $\epsilon$ from Eq. 6 once hydration is measured. The value of $\epsilon$ is then substituted into Eqs. 4 and 5. With the values of $Q$, $\Delta P/L$, $\epsilon$ known, $R$ can then be calculated. The relationship between interstitial spacing $2R$ and native hydration $H$ was fitted to a linear regression line $2R = -0.0375 + 0.0021\ H$, with coefficient of correlation $r = 0.99$ ($P < 0.01$) (Fig. 7). Values of $H$ ranged from 70 to 400, corresponding to solids contents of 1.41 to 0.25%. Calculated values of $2R$ ranged from 0.1–0.8 $\mu$m. Calculated values of $r$ ranged from 40–120 Å.

## DISCUSSION

In this communication we have presented a new approach, involving both theoretical hydrodynamics and experimental measurement, for characterizing microscale properties of cervical mucus and, possibly, other gel systems. By working with the mucus in its native hydrated state, the method is intended to minimize artifacts that may arise when the state is altered before study. Because of the high hydration ($H$) of estrous bovine cervical mucus, the calculations of interstitial ($R$) and filament ($r$) sizes are relatively insensitive to the fine details of the hydrodynamic model. Interfilament interactions are small, and computations based on more sophisticated hydrodynamic analyses would yield very similar results. A second consequence of the high hydration is that the calculation of $r$ and $R$ is relatively insensitive to errors in the experimental measurement of $H$. For example, $R$ is approximately proportional to $[\ln(H^{1/2})]^{1/2}$. Thus a 25% error in the determination of $H = 200$ yields only a 2–3% error in the calculation of $R$.

We suggest that peri-ovulatory bovine cervical mucus contains a macromolecular network characterized by smaller filaments and smaller interstitial sizes than those indicated in earlier studies. It seems likely that this distinction applies to human cervical mucus, as well. Indeed this new characterization of cervical mucus is consistent with the results of recent studies of the direct hydrodynamic interactions between spermatozoa and the mucus (Katz and Berger, 1980). Spermatozoa are, therefore, in very intimate communication with the mucus microstructure, physically as well as electrochemically. This communication undoubtedly plays an important role in the regulation of sperm transport through the cervix (Overstreet and Katz, 1980).

Our study has shown that the mucus permeability increases when the external pressure gradient exceeds 40–60 cm $H_2O$/cm mucus. Indeed, the experimental data display a biphasic pressure-flow relationship (Fig. 2). This biphasic relationship was obtained regardless of the order in which different pressure gradients were applied to a mucus specimen, and, upon repeated testing, no hysteresis was observed. It can, therefore, be surmised that the change in mucus permeability is due to a reversible deformation in the microstructure that resembles a yield-point phenomenon. Such deformation may be of considerable

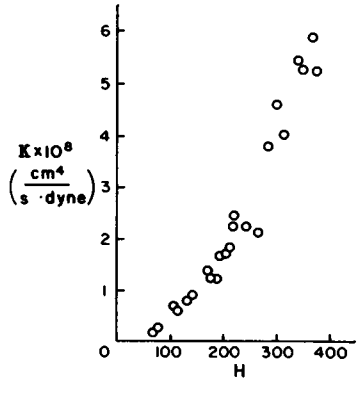


FIGURE 6 Distribution of flow conductivity $k$ at high-pressure regime of flow curve vs. native hydration for bovine cervical mucus.

biological relevance, since pressure differences of the order of 50 cm $H_2O$ may exist across the cervix during the pericoital period (Fox, et al., 1970).

We can suggest two possible interpretations of the biphasic pressure-flow plots. If we assume that the flow conductivity $k$ can be calculated from the local slope of the pressure-flow curve, then two discrete values of $k$ are obtained. These would correspond to two discrete arrangements of the microstructure. Extrapolation of the flow regime of the higher pressure state to below the transition pressure would, however, define a yield pressure below which no flow occurs. Alternatively, strict application of Darcy's Law requires that a zero pressure gradient correspond to zero flow. In this case, the flow conductivity $k$ would continuously increase, even though the slope of the pressure-flow curve remains constant in the higher pressure regime. Denote this regime by the subscript II and the low pressure region by the subscript I. An effective flow conductivity in II can then be defined as

$$Q_{II} = k_{eff} A\Delta P/\eta L. \tag{7}$$

For phase II, $Q_{II} = Q_I + k'A\Delta P/\eta L$, where $k'$ is the flow conductivity evaluated from the local slope of the flow curve in phase II. Let $Q_I = k_0 A\Delta P_T/\eta L = Ak'\Delta P_T/\eta L$ at the transition point of the flow curve. Therefore,

$$Q_{II} = Ak_0\Delta P_T/\eta L + Ak'\Delta P_{II}/\eta L, \tag{8}$$

where $P_T$ is the transition pressure and $\Delta P_{II} + \Delta P_T = \Delta P$. Combining Eqs. 7 and 8,

$$k_{eff} = [k_0\,\Delta P_T + k'\,(\Delta P - \Delta P_T)]/\Delta P. \tag{9}$$

Normalizing $P$ with $\Delta P_T$ and $k_{eff}$ with $k_0$, we have, from Eq. 9,

$$k_{eff}/k_0 = [1 + k'/k_0\,(\Delta P/\Delta P_T - 1)]/(\Delta P/\Delta P_T). \tag{10}$$

A plot of Eq. 10 is shown in Fig. 8. According to this interpretation, the structure of the network is continuously deformed beyond the transition point. The deformation is at first rapid, and approaches a new equilibrium state at pressures beyond three times the transition pressure. Physically this means that the structure is not suddenly changed from one state to another. Rather, there is a more drastic initial deformation which then gradually approaches a new equilibrium configuration.

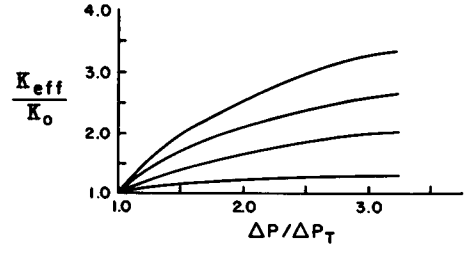


FIGURE 8 Variation of $k_{eff}$ beyond transition pressure in the flow-pressure relationship. $k_{eff}$ is calculated according to Eq. 10 in text.

This study suggests that the interstitial spacing and filament diameter both increase with increasing hydration, i.e., decreasing solids content. The predicted increases in interstitial size with hydration are consistent with inferences drawn from the studies of scanning electron microscopy (e.g. Chretien et al., 1973). Such predicted increases are essentially a hydrodynamic result: as noted previously, $R$ is a weakly increasing function of hydration, cf. Eqs. 4 and 5, but increases as the square root of the flow conductivity, $k$. The concomitant predicted increase in $r$ is necessary to satisfy Eq. 5, i.e., conservation of mass within the mucus. However, it is not certain that there is a continuous increase in actual filament diameters with increasing hydration in native mucus samples. Rather, the increase in effective diameter could be a reflection of conformational changes in the microstructure. The correlation between hydration and mucus rheological properties supports this line of reasoning (Wolf et al., 1977; Tam et al., 1980). Note that for low hydration the permeability is low, i.e., there is a high resistance to flow, cf. Fig. 5. According to the model used in this study, such a higher flow resistance corresponds to a smaller filament diameter, i.e., a finer mesh with a higher number of filaments. However, we must emphasize that our model assumes that the principal resistance to fluid flow within the mucus microstructure is due to viscous drag. Coiled molecules with a nondraining core would also contribute to the overall flow resistance (Tanford, 1961). To the extent that the resistance of such molecules is important, changes in predicted filament size are interpretable as changes in the solvation of the molecules or the incorporation of increased gel into the nondraining region (Weiss and Silberberg, 1977). Thus, our study has determined hydrodynamically equivalent filament sizes with respect to the bulk internal flow.

## APPENDIX

## Hydrodynamic Resistance of a Cubic Lattice

The total hydrodynamic resistance to fluid permeation through a cell is due to the one cylindrical filament whose longitudinal axis is parallel to the direction of flow, and the two filaments with perpendicular axes (Fig. 3). The resistances of these filaments are calculated separately and summed. For the parallel filament, the fluid equations of motion reduce to

$$\eta(d^2u_z/dr^2 + r^{-1}\,du/dr) = dP/dz$$
$$u_z = 0 \text{ at } r = r_0$$
$$du_z/dr = 0 \text{ at } r = R \tag{A1}$$

where $u_z$ is the fluid velocity, which is oriented in the longitudinal $z$-direction only, and $r$ is the radial coordinate in a cylindrical coordinate system. Integrating Eq. A.1

$$u_z = 1/4\eta\,(r^2 - r_0^2 - 2R^2 \ln r/r_0)\,dP/dz. \tag{A2}$$

The fluid drag per unit length, $D_\parallel$, on the filament is given by

$$D_\parallel = 2\pi r_0 \eta (du_z/dr)_{r=r_0} = \pi R^2(\epsilon^2 - 1)\, dP/dz \quad \text{(A3)}$$

where $\epsilon = r_0/R$. Defining the average velocity $U$ as

$$U = 2/R^2 \int_{r_0}^{R} r u_z \, dr \quad \text{(A4)}$$

and substituting in Eqs. A2 and A3, we obtain

$$D_\parallel = 2\pi\eta U(1 - \epsilon^2)/[\ln(1/\epsilon) + \epsilon^2 - \epsilon^4/4 - 0.75]. \quad \text{(A5)}$$

The fluid drag on a perpendicular filament is obtained via an analogous calculation. In this case, the fluid drag $D_\perp$ per unit length is obtained as

$$D_\perp = 4\pi\eta U/[\ln(1/\epsilon) + \epsilon^2 - \epsilon^4/4 - 0.75]. \quad \text{(A6)}$$

Now the total drag on a fluid cell is $\mathcal{D} = 2R(D_\parallel + 2D_\perp)$, so that

$$\mathcal{D} = 4\pi\eta RU\{(5 - \epsilon^2)/[\ln(1/\epsilon) + \epsilon^2 - \epsilon^4/4 - 0.75]\}. \quad \text{(A7)}$$

This is balanced by the pressure difference $\Delta P$ across the cell, i.e.,

$$\mathcal{D} = \pi\Delta P(R^2 - r_0^2). \quad \text{(A8)}$$

Noting that $dP/dz = \Delta P/L$, where $L$ is the length of the cell, and that $L = 2R$, combination of Eqs. A4, A7, and A8 yields

$$R^2 = 2\eta U(1 - \epsilon^2)^{-1}\{(5 - \epsilon^2)/[\ln(1/\epsilon) + \epsilon^2 - \epsilon^4/4 - 0.75]\}(\Delta P/L)^{-1}. \quad \text{(A9)}$$

In the permeation experiments $\Delta P/L$ is equal to the net pressure drop across the mucus plug divided by the length of the plug; $U$ is approximately equal to $Q/A$, where $Q$ is the measured net volume flux of fluid expressed from the mucus plug, and $A$ is the cross-sectional area of the plug.

## Determination of $\epsilon$

An expression for $\epsilon$ can be obtained by using the fluid cell model previously described. The procedure involves experimental determination of hydration $H$ (weight of water per weight of solid). $\epsilon$ can be related to $H$ by the following theoretical model (Fig. 4):

$$\text{Total volume of fluid cell} = \pi R^2 L = 2\pi R^3. \quad \text{(A10)}$$

$$\text{Volume of solid in cell} = 3\pi r_0^2 L = 6\pi r_0^2 R.$$

$$\text{Volume of fluid} = \text{Eqs. A10–A11} = 2\pi R(R^2 - 3r_0^2)$$

$$H = \text{weight of water/weight of solid} = \rho_f \times \text{volume of fluid}/\rho_s \times \text{volume of solid}; \quad \text{(A11)}$$

$\rho_f$, $\rho_s$ are the densities of the fluid and solid, respectively.

To first approximation, assume $\rho_f = \rho_s$ (Cohn and Edsall, 1943). We have then

$$H = \pi R(R^2 - 3r_0^2)/(3\pi r_0^2 R) = (3\epsilon^2)^{-1} - 1 \quad \text{(A12)}$$

$$\epsilon = [3(H + 1)]^{-1/2}. \quad \text{(A13)}$$

The value of $\epsilon$ is calculated from Eq. A13 once the value of $H$ is determined experimentally.

We thank Prof. I. Fatt, School of Optometry, University of California, Berkeley, for his many helpful suggestions, and Prof. J. W. Kendrick and R. Bon Durant, Department of Reproduction, School of Veterinary Medicine, University of California, Davis for the collection of the mucus samples.

Dr. Tam is the recipient of a National Institutes of Health (NIH) Bioengineering Traineeship; Dr. Katz received NIH grant HD12971.

*Received for publication 16 April 1980 and in revised form October 1981.*

## REFERENCES

Blandau, R. J., and K. Moghissi. 1973. The Biology of the Cervix. University of Chicago Press, Chicago. 1–450.

Chretien, F. 1977. Technical problems involving scanning electron microscopic observation of cervical mucus framework. *In* The Uterine Cervix in Reproduction. V. Insler and G. Bettendorf, editors. G. Thieme Publishers, Stuttgart. 45–51.

Chretien, F., C. Cernigon, C. David, and A. Psychoyos. 1973. The ultrastructure of human cervical mucus under scanning electromicroscopy. *Fertil. Steril.* 24:746–757.

Cohn, E. D., and J. W. Edsall. 1943. Protein, Amino Acids and Peptides. Hafner Publishing Company, New York.

Davajan, V., R. M. Nakamura, and K. Kharma. 1970. Spermatozoan transport in cervical mucus. *Obstet. Gynecol. Survey.* 25:1–43.

Eliezer, N. 1974. Viscoelastic properties of mucus. *Biorheology.* 11:61–68.

Elstein, M., K. Moghissi, and R. Berth. 1973. Cervical Mucus in Human Reproduction. Scriptor, Ltd., Copenhagen, 1–163.

Fox, C. A., H. S. Wolff, and J. A. Baker. 1970. Measurement of intra-vaginal and intra-uterine pressures during human coitus by radio-telemetry. *J. Reprod. Fertil.* 22:243–251.

Gibbons, R. A., and P. E. Mattner. 1966. Some aspects of the chemistry of cervical mucus. *Int. J. Fertil.* 11:366–372.

Gibbons, A., and P. E. Mattner. 1971. The chemical and physical class of the cervical secretion and the role in reproductive physiology. *In* Pathways to Conception. A. I. Sherman, editor. Charles C. Thomas Publisher, Springfield, IL. 143–155.

Katz, D. F., and J. R. Singer. 1978. Water mobility within bovine cervical mucus. *Biol. Reprod.* 17:843–849.

Katz, D. F., and S. A. Berger. 1980. Flagellar propulsion of human sperm in cervical mucus. *Biorheology.* 17:169–175.

Lutz, R. J., M. Litt, and L. W. Chakrin. 1973. Physical-chemical factors in mucus rheology. *In* Rheology of Biological Systems. H. L. Gabelnick and M. Litt, editors. Charles C. Thomas Publisher, Springfield, IL. 119–157.

Nakamura, R. M., V. Davajan, M. Saga, and S. E. Allerton. 1973. Salient biophysical properties of cervical mucus. *In* Cervical Mucus in Human Reproduction. Scriptor, Ltd., Copenhagen. 75–81.

Overstreet, J. W., and D. F. Katz. 1977. Sperm transport and selection in the female genital tract. *In* Mammalian Development. M. H. Johnson, editor. Elsevier/North-Holland, Amsterdam. 31–65.

Overstreet, J. W., and D. F. Katz. 1980. Sperm transport, capacitation. *In* Gynecology and Obstetrics. V. Reproductive Endocrinology, Infertility and Genetics. L. Speroff, and J. L. Simpson, editors. Harper & Row Publishers, New York.

Singer, A., and B. L. Reid. 1970. Effect of oral contraceptive steroids on the ultrastructure of human cervical mucus. A preliminary communication. *J. Reprod. Fertil.* 23:249–255.

Tam, P. Y., D. F. Katz, and S. A. Berger. 1980. Non-linear viscoelastic properties of cervical mucus. *Biorheology.* 17:465–478.

Tanford, C. 1961. Physical Chemistry of Macromolecules. John Wiley & Sons, New York.

van Bruggen, E. F. J., and J. Kremer. 1970. Electron microscopy of bovine and human cervical mucus. *Int. J. Fertil.* 15:50–57.

Weiss, N., and A. Silberberg. 1977. Inhomogeneity of polyacrilamide gel

structure from permeability and viscoelasticity. *Br. Polymer J.* 9:144–150.

Wolf, D. P., L. Blasco, M. Khan, and M. Litt. 1977. Human cervical mucus. I. Rheological characteristics. *Fertil. Steril.* 28:41–46.

Yaron, I., and B. Gal-Or. 1971. Convective mass and heat transfer from size-distributed drops, bubbles or solid particles. *J. Heat Mass Trans.* 14:727–737.

Zaneveld, L. J. D., P. F. Tauber, C. Port, D. Propping, and G. F. B. Schumaker. 1975. Structural aspects of human cervical mucus. *Am. J. Obstet. Gynecol.* 122:650–654.